



## Preliminary characterization of the upper haze by SPICAV/SOIR solar occultation in UV to mid-IR onboard Venus Express

V. Wilquet,<sup>1</sup> A. Fedorova,<sup>2</sup> F. Montmessin,<sup>3,4</sup> R. Drummond,<sup>1</sup> A. Mahieux,<sup>1</sup>  
A. C. Vandaele,<sup>1</sup> E. Villard,<sup>3,4</sup> O. Korablev,<sup>2</sup> and J.-L. Bertaux<sup>3,4</sup>

Received 9 May 2008; revised 19 January 2009; accepted 22 April 2009; published 10 July 2009.

[1] The Spectroscopy for Investigation of Characteristics of the Atmosphere of Venus/Solar Occultation at Infrared (SPICAV/SOIR) suite of instruments onboard the Venus Express spacecraft comprises three spectrometers covering a wavelength range from ultraviolet to midinfrared and an altitude range from 70 to >100 km. However, it is only recently (more than 1 year after the beginning of the mission) that the three spectrometers can operate simultaneously in the solar occultation mode. These observations have enabled the study of the properties of the Venusian mesosphere over a broad spectral range. In this manuscript, we briefly describe the instrument characteristics and the method used to infer haze microphysical properties from a data set of three selected orbits. Discussion focuses on the wavelength dependence of the continuum, which is primarily shaped by the extinction caused by the aerosol particles of the upper haze. This wavelength dependence is directly related to the effective particle radius (cross section weighted mean radius) of the particles. Through independent analyses for the three channels, we demonstrate the potential to characterize the aerosols in the mesosphere of Venus. The classical assumption that the upper haze is only composed of submicron particles is not sufficient to explain the observations. We find that at high northern latitudes, two types of particles coexist in the upper haze of Venus: mode 1 of mean radius  $0.1 \leq r_g \leq 0.3 \mu\text{m}$  and mode 2 of  $0.4 \leq r_g \leq 1.0 \mu\text{m}$ . An additional population of micron-sized aerosols seems, therefore, needed to reconcile the data of the three spectrometers. Moreover, we observe substantial temporal variations of aerosol extinction over a time scale of 24 h.

**Citation:** Wilquet, V., A. Fedorova, F. Montmessin, R. Drummond, A. Mahieux, A. C. Vandaele, E. Villard, O. Korablev, and J.-L. Bertaux (2009), Preliminary characterization of the upper haze by SPICAV/SOIR solar occultation in UV to mid-IR onboard Venus Express, *J. Geophys. Res.*, *114*, E00B42, doi:10.1029/2008JE003186.

### 1. Introduction

[2] Venus is completely enshrouded in clouds which show an enormous vertical extent of more than 50 km. Venus' clouds are mainly found in a cloud deck located between 45 and 70 km of altitude, with thin hazes above and below. Much of the clouds are composed of H<sub>2</sub>SO<sub>4</sub> aerosol particles showing a multimodal particle size distribution. The upper haze (70–90 km) is composed of submicron aerosol particles with an effective radius below  $0.3 \mu\text{m}$  [Lane and Opstbaum, 1983; Sato *et al.*, 1996]. The composition of these particles was derived from the Pioneer Venus Orbiter Cloud photopolarimeter experiment [Kawabata *et al.*, 1980]. A refractive index of 1.4 was measured, which is in agreement with a haze consisting of

concentrated sulfuric acid (75%). Kawabata *et al.* [1980] showed that the haze is thicker at high latitudes and very diffuse in the tropics. Larger particles are found at lower altitudes. Particles with a mean radius of about  $1.0 \mu\text{m}$  are the principal constituent of the main cloud deck. Even bigger particles with a mean radius larger than  $4.0 \mu\text{m}$  have been observed at levels below the tropopause.

[3] The Spectroscopy for Investigation of Characteristics of the Atmosphere of Venus (SPICAV) instrument [Bertaux *et al.*, 2007], which is composed of three independent spectrometers, namely the UV and IR spectrometers and the Solar Occultation at Infrared (SOIR) instrument, was developed in view of investigating the Venus atmosphere from the ground up to the uppermost limit of the atmosphere. Each channel of the instrument can perform, vertical profiling by mean of solar occultation, this is the first time at Venus. Besides the detection of CO<sub>2</sub>, H<sub>2</sub>O, and HDO, as well as other minor constituents, this instrument provides unrivalled information on the aerosol loading of the atmosphere. Taken separately all three channels, operating in the solar occultation mode, can contribute to the characterization of the aerosol extinction as well as, in some cases, of

<sup>1</sup>Belgian Institute for Space Aeronomy, Brussels, Belgium.

<sup>2</sup>Space Research Institute, Moscow, Russia.

<sup>3</sup>Service d'Aéronomie du CNRS, Verrières-le-Buisson, France.

<sup>4</sup>Institut Pierre Simon Laplace, Université de Versailles Saint Quentin, Guyancourt, France.

the aerosol particle size. We will show that if we combine their measurements, it is moreover possible to define a bimodal distribution of the aerosol particles size. This information is of great interest as it is known that aerosol particles, through absorption and scattering of solar radiation, play a major role in the energetic balance of the atmosphere.

## 2. SPICAV/SOIR Instrument

[4] SPICAV is a suite of three spectrometers in the UV and IR range dedicated to the study of the atmosphere of Venus from ground level to the outermost hydrogen corona at more than 40,000 km. It is derived from the SPICAM instrument flying on board Mars Express (MEX), with the addition of a new IR high-resolution spectrometer SOIR [Bertaux *et al.*, 2007]. The UV spectrometer (118–320 nm, resolution 1.5 nm) is identical to the MEX version. It is dedicated to nadir viewing, limb viewing and vertical profiling by stellar and solar occultation. The SPICAV IR sensor (0.65–1.7  $\mu\text{m}$ , resolution 0.5–1.2 nm) which makes use of an Acoustooptical tunable filters (AOTF), investigates the dayside solar radiation reflected from the clouds and the nightside thermal emission coming through the clouds in nadir mode, and in solar occultation mode, this channel studies the vertical profiles of  $\text{H}_2\text{O}$ ,  $\text{CO}_2$ , and aerosols. The pioneer SOIR spectrometer is a solar occultation IR spectrometer with the highest spectral resolution on board VEX. This new concept of instrument includes a combination of an echelle grating and an AOTF crystal to select one order at a time. One of the main objectives of SOIR is to measure HDO and  $\text{H}_2\text{O}$  in solar occultation [Bertaux *et al.*, 2007; Fedorova *et al.*, 2008a; Svedhem *et al.*, 2007], in order to characterize the escape of D atoms from the upper atmosphere and give more insight about the evolution of water on Venus. However, the instrument is also well adapted to investigate the isotopologues of  $\text{CO}_2$  [Bertaux *et al.*, 2008; Wilquet *et al.*, 2008] and other minor species [Vandaele *et al.*, 2008]. The three channels of the SPICAV/SOIR instrument will be described in the following sections more specifically in view of their capabilities to characterize the aerosols present in the Venus atmosphere. The instrument is on the Venus Express spacecraft operating on the orbit around Venus from April 2006. This orbit lasts about 24 h and is highly elliptical with nearly 80°N pericenter [Titov *et al.*, 2006]. The vertical resolution of the occultation is better when the distance to the limb is small, which is the case, for such an elongated orbit, at high northern latitudes.

### 2.1. UV Channel

[5] The ultraviolet channel of SPICAV is a versatile instrument, operating in a wide range of modes: nadir, limb, and solar/stellar occultations. A detailed instrument description can be found in the paper by Bertaux *et al.* [2007]. The UV channel covers the 118 to 320 nm spectral range with a spectral sampling of 0.54 nm per pixel while the actual spectral resolution determined by optical aberration is three pixels (i.e.,  $\sim 1.5$  nm). The UV channel is a compact imaging spectrometer equipped with an image intensifier and a Thomson CCD array of  $288 \times 384$  pixels.

[6] The focal length of the UV telescope is such that one CCD pixel covers a field of view (FOV) of  $0.01 \times 0.01^\circ$ . The total useful FOV of the instrument is, however, limited by a slit located in the focal plane, whose width equals two CCD pixels as imposed by Nyquist-Shannon sampling theorem. Total FOV varies between  $0.02^\circ \times 0.1^\circ$  and  $0.02^\circ \times 0.4^\circ$  depending on CCD readout configuration.

[7] Owing to downlink limitations, the equivalent of only 5 out of the 288 available pixel lines can be transmitted to Earth. To comply with this restriction while making use of a larger portion of the photosensitive area, pixel lines are first binned together during readout. The number of lines per bin (also referred to as bands) is determined upon consideration of photometry. For solar occultations, five adjacent bins of two to eight lines are used. In order to maintain the same vertical resolution at the limb of  $\sim 1$  km, a particular combination of integration time (ranging between 80 and 450 ms) and line binning (from two to eight) is set to adjust with the altitude of the spacecraft during solar occultation. See the numerous articles describing the binning procedure in more detail [Bertaux *et al.*, 2007; Montmessin *et al.*, 2006a, 2006b; Quémerais *et al.*, 2006].

[8] The signal-to-noise ratio (SNR) has been determined by observing the sun outside the atmosphere where the signal is stable and varies only according to photon statistical noise. This analysis showed that pixel SNR can exceed 150 ( $\text{SNR}_{\text{max}}$ ) in the range 200 to 300 nm for a single measurement. Below 200 nm, solar emission drops rapidly and yields no detector count shortward of 170 nm. As the line of sight traverses progressively deeper regions of the atmosphere, SNR decreases as  $\text{SNR}_{\text{max}} \times (\exp(-\tau))^{1/2}$  where  $\tau$  is the slant opacity of the atmosphere.

[9] UV data treatment is performed through a succession of steps. First, dark charge (DC) and offset are subtracted from pixel content using masked pixels located at the extremity of each pixel line and dedicated to dark charge estimation. A predetermined non uniformity pattern allows extraction of an instantaneous DC value for any pixel of the CCD from reading of the masked CCD pixels. In addition, when a significant portion of the occultation sequence remains behind Venus with respect to the sun, i.e., SPICAV line of sight aims at Venus nightside, the electronic readout noise pattern (with a periodicity of 14 pixels) can be isolated and subtracted throughout the sequence, thereby improving the scientific analysis of low-statistics signals.

[10] Atmospheric transmission spectrum is computed as the ratio of the spectrum collected at a given altitude to the reference spectrum of the sun formed by coadding hundreds of solar spectra recorded outside the atmosphere (Figure 1a.).

[11] On some sequences, the solar spectrum recorded outside the atmosphere shows a linear drift of the signal amplitude throughout the sequence. The cause of this drift is still not clearly established but appears related to center-to-limb darkening effect of the sun. Intensity variation is then produced by spacecraft line of sight scanning across the solar disk as a result of either the spacecraft slewing in one direction or, most likely, the orbital course of the spacecraft itself projecting at different locations at the surface of the sun. In any case, this effect is corrected for by performing a linear regression of the solar signal variation outside the atmosphere and by extrapolating the linear variation to the reference spectrum over the whole sequence.

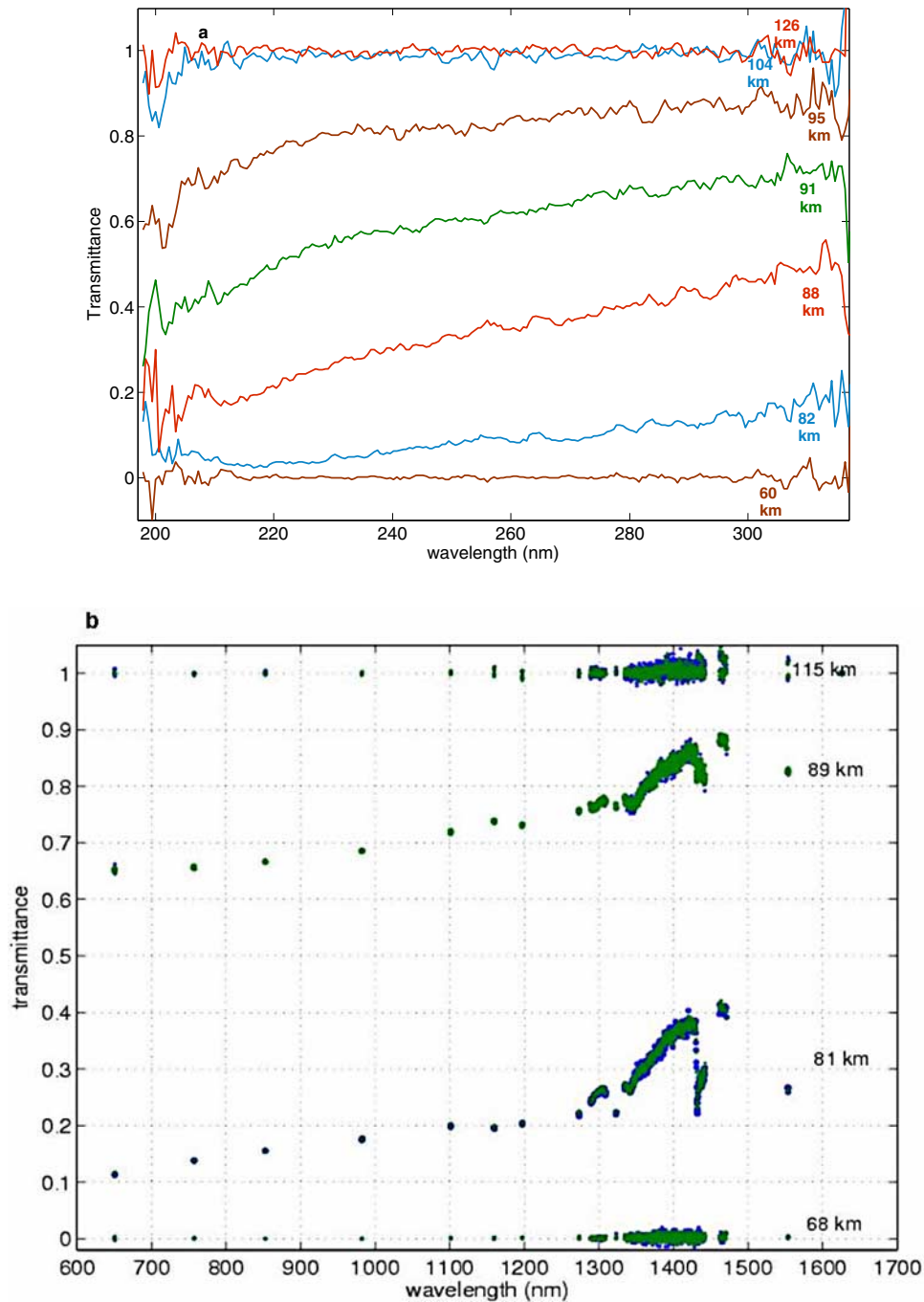


**Figure 1.** Example of transmittance spectra for the three channels during occultation 486. (a) SPICAV-UV: transmittance at several altitudes during the occultation. (b) SPICAV-IR: sequential scanning of 664 spectral points recorded by defining three windows (spectral ranges 1288.5–1309.3 nm, 1334.4–1442.5 nm, and 1461.5–1471.1 nm) and 11 individual measurements described as “dots” (wavelengths 650.8, 757.2, 852.7, 982.3, 1101.1, 1159.6, 1197.2, 1273.5, 1323.0, 1553.7, and 1626.0 nm). Last dot is not used for the retrieval owing to its sensitivity to a CO<sub>2</sub> absorption band. (c) SOIR: a series of transmittances throughout the occultation. Each image corresponds to one selected diffraction order (spectral window).

## 2.2. Near-IR Channel

[12] The SPICAV-IR instrument is part of the SPICAV/SOIR experiment on board the Venus Express mission. It is a new generation of the AOTF spectrometer (SPICAM-IR) on MEX [Fedorova *et al.*, 2008b; Korablev *et al.*, 2006].

SPICAV-IR works in the range 0.65–1.7  $\mu\text{m}$  with a spectral resolution of 5.2  $\text{cm}^{-1}$  in the LWL channel (1–1.7  $\mu\text{m}$ ) and 7.8  $\text{cm}^{-1}$  in the SWL channel (0.6–1.05  $\mu\text{m}$ ). Two photodiodes register light in the two orthogonal polarizations at the AOTF output. The spectrometer is designed to work in



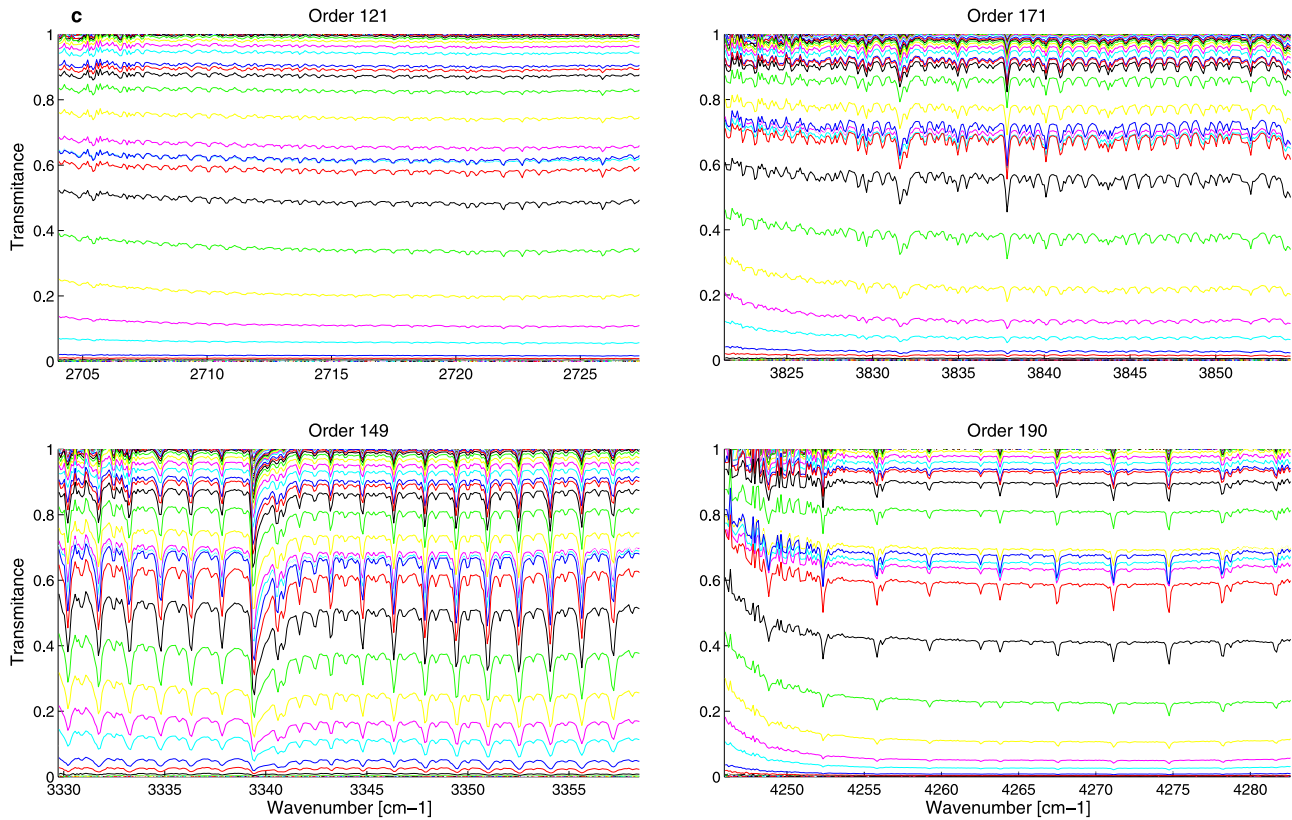


Figure 1. (continued)

nadir or solar occultation mode. The entry optics (a small lens with an useful diameter of 3 mm and a circular diaphragm) provides an angular field of view of about  $4'$  or  $0.07^\circ$  for solar occultation observations, which corresponds to a vertical resolution of 1–15 km on the limb of Venus, depending on the spacecraft altitude. SPICAV-IR works on the principle of sequential scanning of the spectrum. Each spectral point is recorded in 2.8 ms. To shorten the spectrum recording time to 2 s (664 spectral points), a regime of “windows” and “dots” has been used (Figure 1b) [see also Korabev *et al.*, 2006]. First, the instrument scans the spectral windows (from longer wavelength downward) then the reference wavelengths are recorded in reversed order. In solar occultation mode, the possible windows are 1461.5–1471.1 nm, 1334.4–1442.5 nm and 1288.5–1309.6 nm, primarily dedicated to measurements of  $\text{CO}_2$  and  $\text{H}_2\text{O}$  abundances from the  $1.43 \mu\text{m}$  and  $1.38 \mu\text{m}$  bands, respectively. Aerosol properties and vertical distributions are determined using 10 continuum points outside the gas absorption bands (Figure 1b).

### 2.3. SOIR Channel

[13] The instrument [Bertaux *et al.*, 2007; Nevejans *et al.*, 2006] and its in-flight performances [Mahieux *et al.*, 2008], including data handling, onboard background subtraction, calibrations of the AOTF and the echelle spectrometer, have already been extensively described, whereas the retrieval technique and some results are discussed in the paper by Vandaele *et al.* [2008]. SOIR is an echelle grating spectrometer operating in the IR, combined with an AOTF for the selection of the diffraction grating orders. It is designed

to measure the atmospheric transmission in the IR ( $2.2\text{--}4.3 \mu\text{m}$ ) at high resolution ( $0.15 \text{ cm}^{-1}$ ), using the method of solar occultation (Figure 1c).

[14] The SOIR detector has 320 columns along the wave number axis and 256 rows along the spatial axis. To avoid saturation, short integration times are used (20 to 30 ms), depending on the wavelength at which the measurement is taken. The background signal is measured and subtracted onboard. In order to improve the signal-to-noise ratio (SNR), a number of measurements can be accumulated as long as the total measuring time remains below 250 ms.

[15] The slit height is 30 arc min and it is projected onto 32 rows of the detector. The slit width is equivalent to 2 detector pixels in the spectral direction. The spectral resolution of the spectrometer is very high and varies between  $0.13 \text{ cm}^{-1}$  at  $4.0 \mu\text{m}$  (order 111) and  $0.27 \text{ cm}^{-1}$  at  $2.3 \mu\text{m}$  (order 192). The corresponding resolving power [ $\lambda/\Delta\lambda = \nu/\Delta\nu$ ] exceeds 20,000 [Mahieux *et al.*, 2008].

[16] Owing to telemetry limitations, only eight spectra, each 320 pixels long, can be downloaded per second. During most observations of Venus, these eight spectra are taken in four different diffraction orders (four different RFs applied to the AOTF), each corresponding to two large bins of 16 or 12 rows on the detector.

### 3. Data Sets and Observation Strategy

[17] Figure 2 shows the spatial distribution of all solar occultations performed by the three channels of SPICAV/SOIR since March 2007, i.e., since it was rendered possible to perform simultaneous observations for SOIR and SPI-

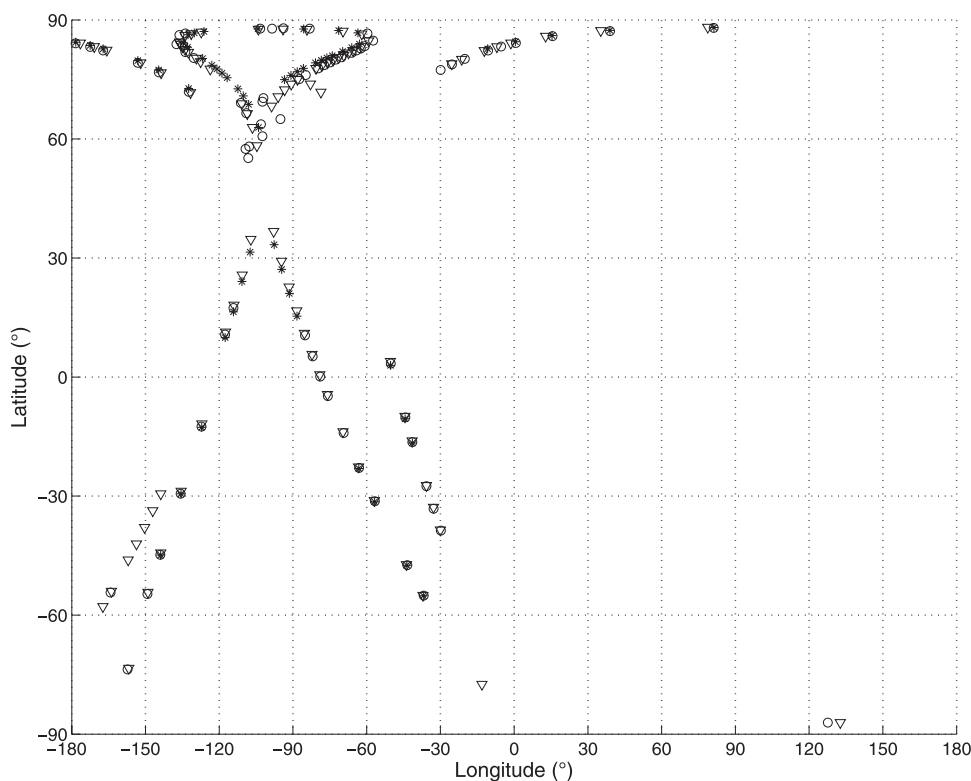


**Figure 2.** Spatial map of measurements in the solar occultation mode, acquired since March 2007, for the three channels of the SPICAV/SOIR instrument. Coordinates of the limb tangent points at an altitude of 120 km for SPICAV-UV (circles), SPICAV-IR (inverted triangles), and SOIR (asterisks).

CAV in the solar occultation mode. This paper is aimed at demonstrating the capability of the instrument to sound the vertical structure of aerosols in the upper haze through occultation spectroscopy. We will therefore concentrate on a few observations for which we had simultaneous data for the three channels (see Table 1). The line of sight to the Sun is slightly different for the three channels so that the portion of the atmosphere probed is not exactly the same, yet the geophysical positions of the tangent point (the point along the optical path that is the closest to the surface of the planet) are very close. The analysis of the data sets from each channel of the instrument is made independently in order to eliminate any instrumental issues. All these observations are located at high northern latitudes (between  $+60^\circ$  and  $+75^\circ$ ).

[18] During a solar occultation, e.g., for a sunset, the measurement cycle is started before the instrument's line of sight intersects with the top layers of the atmosphere, and a reference spectrum can be recorded for each channel. Below that level, solar light is absorbed by atmospheric components and the intensity of the recorded signal starts to decrease. As spectra obtained during the occultation are divided by the reference solar spectrum recorded outside the atmosphere, any solar or instrumental signature gets removed and the transmittance contains only information about the Venus atmosphere. This is illustrated in Figure 1c where the transmittances obtained during occultation 486 for 4 different spectral windows centered at  $\sim 2715$ , 3343, 3838, and  $4264 \text{ cm}^{-1}$  (orders 121, 149, 171, and 190) are plotted. The evolution of the light transmission during solar

occultation 485 is depicted in Figure 3 for the three channels of the SPICAV/SOIR instrument: two wavelengths for the UV channel, two wavelengths for the IR channel, and the average signal for two diffraction orders recorded during this occultation for SOIR. The vertical resolution depends on the geometry of the solar occultations and the distance to the limbs of VEX. In the orbits analyzed in this paper the vertical resolution is  $\sim 3.0 \text{ km}$  for SPICAV-UV,  $\sim 3.4 \text{ km}$  for SPICAV-IR, and  $\sim 2.0 \text{ km}$  for SOIR.

## 4. Method of Analysis

### 4.1. Retrieval of the Extinction Coefficients

[19] All three instruments, taken together, provide useful information on the absorption due to aerosols. In this section, we will first indicate how aerosol extinction coefficients are obtained from the measurements, which are

**Table 1.** Distance to the Limb, Longitude, and Latitude for Each Orbit at a Tangent Height of 65 km and 120 km Showing How These Values Vary During the Occultation

Orbit	Date	Distance to the limb (km)		Longitude (deg)		Latitude (deg)	
		65 km	120 km	65 km	120 km	65 km	120 km
482	16 Aug 2007	2474	2131	242	243	+73	+75
484	18 Aug 2007	2657	2277	246	248	+70	+73
485	9 Aug 2007	2790	2380	249	250	+68	+71
486	20 Aug 2007	2973	2515	251	252	+65	+69
487	21 Aug 2007	3249	2702	253	254	+61	+66

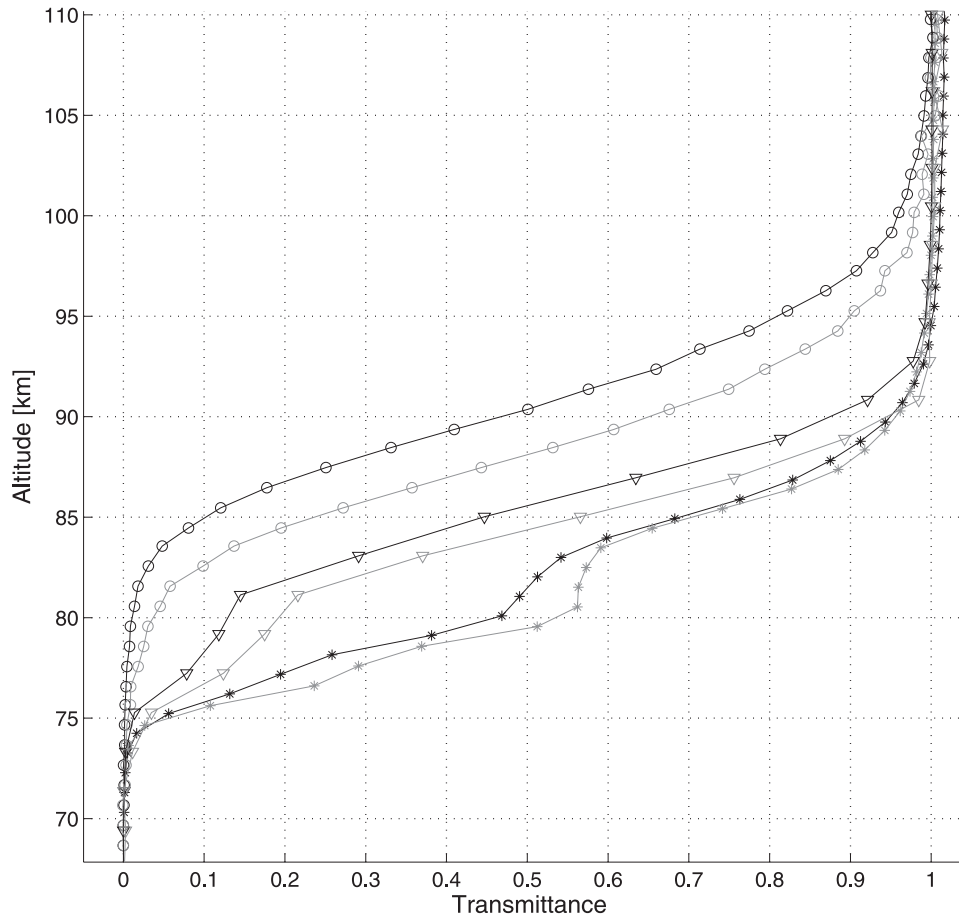


**Figure 3.** Solar light transmission through the Venus atmosphere of the solar occultation performed during orbit 485 by the SPICAV/SOIR instrument. Two wavelengths for each channel are plotted here: SPICAV-UV at 220 nm (black circles), SPICAV-UV at 300 nm (gray circles), SPICAV-IR at 757 nm (black inverted triangles), SPICAV-IR at 1553 nm (gray inverted triangles), SOIR at 2560 nm (black asterisks), and SOIR at 3978 nm (gray asterisks).

different in kind for the three channels of the instrument. Then we will investigate how particle size and number density can be inferred from these measurements.

#### 4.1.1. UV Channel

[20] The inversion procedure is almost identical to the one applied to the SPICAM stellar occultations at Mars, with the exception that solar occultations provide a narrower spectral range to extract the CO<sub>2</sub> concentration. The reader is therefore referred to the numerous publications dedicated to the subject [Montmessin *et al.*, 2006a, 2006b; Quémerais *et al.*, 2006]. Inverting occultation data only requires consideration of the simple Beer-Lambert's law, which states that source attenuation scales exponentially with opacity. Spectral inversion is performed independently for every altitude. For every level, a least squares fitting technique (Levenberg-Marquardt) is used to infer the amount of CO<sub>2</sub>, which possesses a prominent electronic transition between 120 and 200 nm, and the aerosol opacity; both quantities being integrated over the line of sight. Profiles of CO<sub>2</sub> local density and aerosol local extinction ( $\beta$ ) are obtained after vertical inversion using Abel's integrals.

[21] For each integration, five spectra are recorded simultaneously by the instrument, each corresponding to a distinct position relative to the limb. Each band of the

detector therefore provides an independent profiling of the atmosphere. However, it was found in a number of cases (usually when the spacecraft was far from the limb) that a significant shift existed between the transmission profiles of each band. This was most likely caused by a relative error of altitude registration between the pixels of the CCD. A 5-point boxcar average has therefore been applied to the aerosol profiles to smooth out the scatter of values.

#### 4.1.2. SPICAV IR and SOIR Channels

[22] The first step is to determine the extinction ( $\beta$ ) in each atmospheric layer, supposed to be homogenous, where we have a measurement by using an onion-peeling method [Vandaele *et al.*, 2008] and by assuming that  $\int \beta dz = -\ln(T)$  where  $T$  is the observed transmittance from which line absorptions have been removed, and  $dz$  is the thickness of the layer under consideration. Cumulative and local extinction coefficients were retrieved from each of the series of transmittances recorded during one occultation: the values correspond to the average value of the signal, for SOIR, in each selected diffraction order and, for SPICAV IR, for each selected spectral point. Except for some details due to the instrument specificity, the inversion procedure for SPICAV-IR is identical to the one described for the SPICAM solar occultations on Mars [Fedorova *et al.*, 2008b].

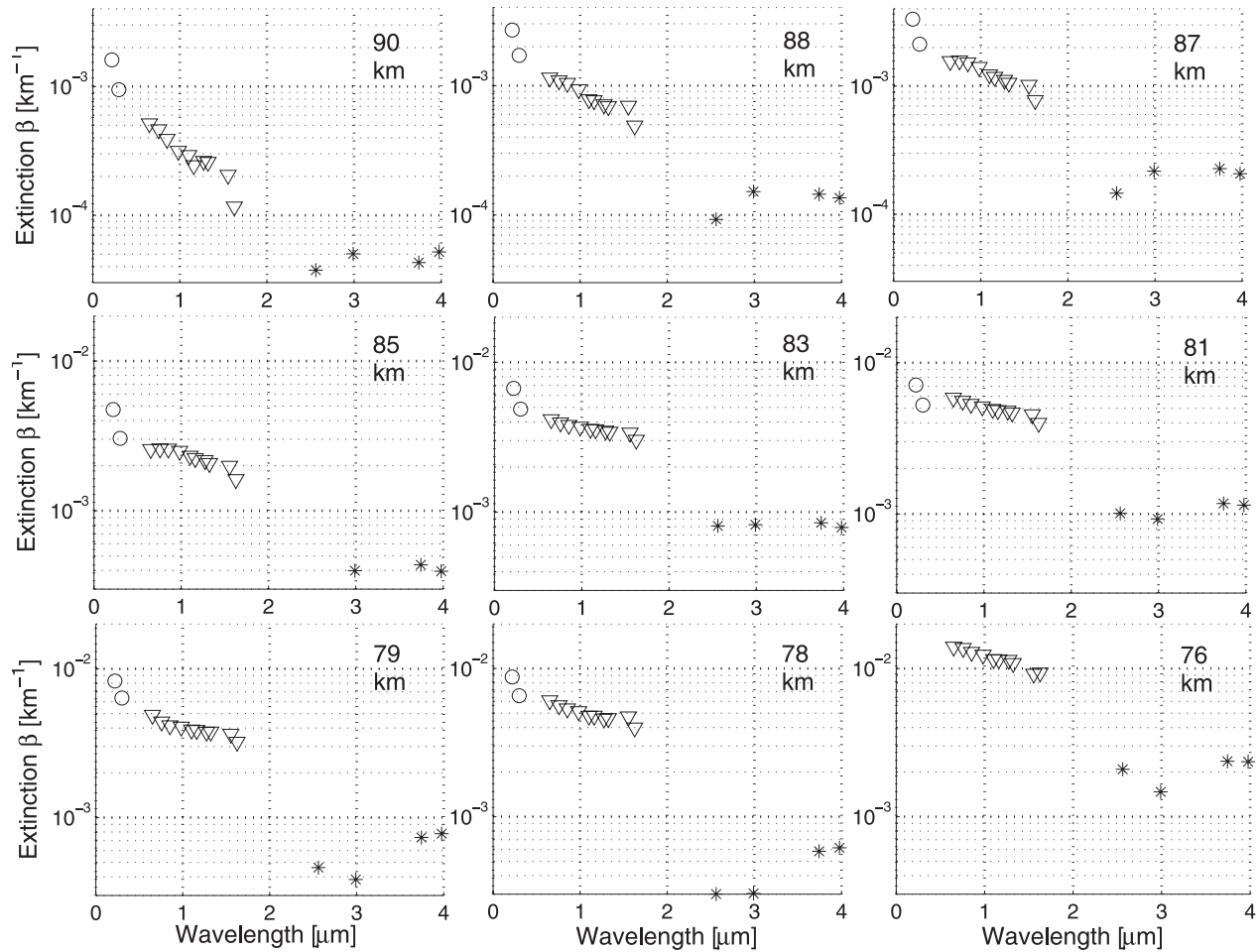


**Figure 4.** Spectral dependence of the extinction coefficient  $\beta$  during orbit 485. The extinction was obtained from data acquired at two wavelengths with the SPICAV-UV channel (circles), at 10 wavelengths with the SPICAV IR channel (inverted triangles), and at four wavelengths with the SOIR channel (asterisks). The various altitudes of the solar occultation are mentioned in the top right corner.

#### 4.1.3. Spectral Dependence

[23] First, we investigate the spectral dependence of the extinction for the different wavelengths probed by the instrument. The extinction coefficients deduced, as explained earlier, from the measurements performed by the three channels are plotted as a function of wavelength in Figure 4, for various altitudes of solar occultation performed during orbit 485.

[24] The Angström exponent ( $\alpha$ ) is usually used to describe the dependency of the aerosol extinction coefficient on wavelength:

$$\beta = \beta_0 \left( \frac{\lambda}{\lambda_0} \right)^{-\alpha} \quad (1)$$

[25] In the case of the UV channel only two points are shown to facilitate reading. The spectral dependence follows a power law (see Table 2). Usually, all the other points fall in between the two plotted points, defining a clear spectral dependence which allows the unambiguous determination of the particle size, see thereafter.

[26] The SPICAV near-IR data also exhibit an obvious spectral dependency, while the spectral dependency of the

aerosol extinction for the SOIR data is slight and not monotonic, and therefore is not described by equation (1). The occultations chosen for this paper are selected so that the 4 spectral windows probed by SOIR are well spread over its entire spectral range, in order to maximize the aerosol extinction variations in function of the wavelength (Figure 4).

#### 4.2. Determination of the Radius and of the Total Number Density of the Particles

[27] The extinction coefficient is expressed as

$$\beta(z; \lambda) = \int_0^{+\infty} N(z) f(r) Q(r; \lambda) dr \quad (2)$$

**Table 2.** Values of the Angström Exponent in the Near-IR and in the UV for Various Sizes of Particles

$r$ ( $\mu\text{m}$ )	$\lambda = 0.3 \mu\text{m};$	$\lambda = 0.75 \mu\text{m};$	$\lambda = 1.00 \mu\text{m};$	$\lambda = 1.55 \mu\text{m};$
	$\lambda_0 = 0.2 \mu\text{m}$	$\lambda_0 = 0.85 \mu\text{m}$	$\lambda_0 = 0.85 \mu\text{m}$	$\lambda_0 = 0.85 \mu\text{m}$
0.2	2.3	2.07	2.4	2.8
0.7	$\sim 0$	-0.65	-0.48	0.12
1.0	$\sim 0$	-0.3	-0.56	-0.50



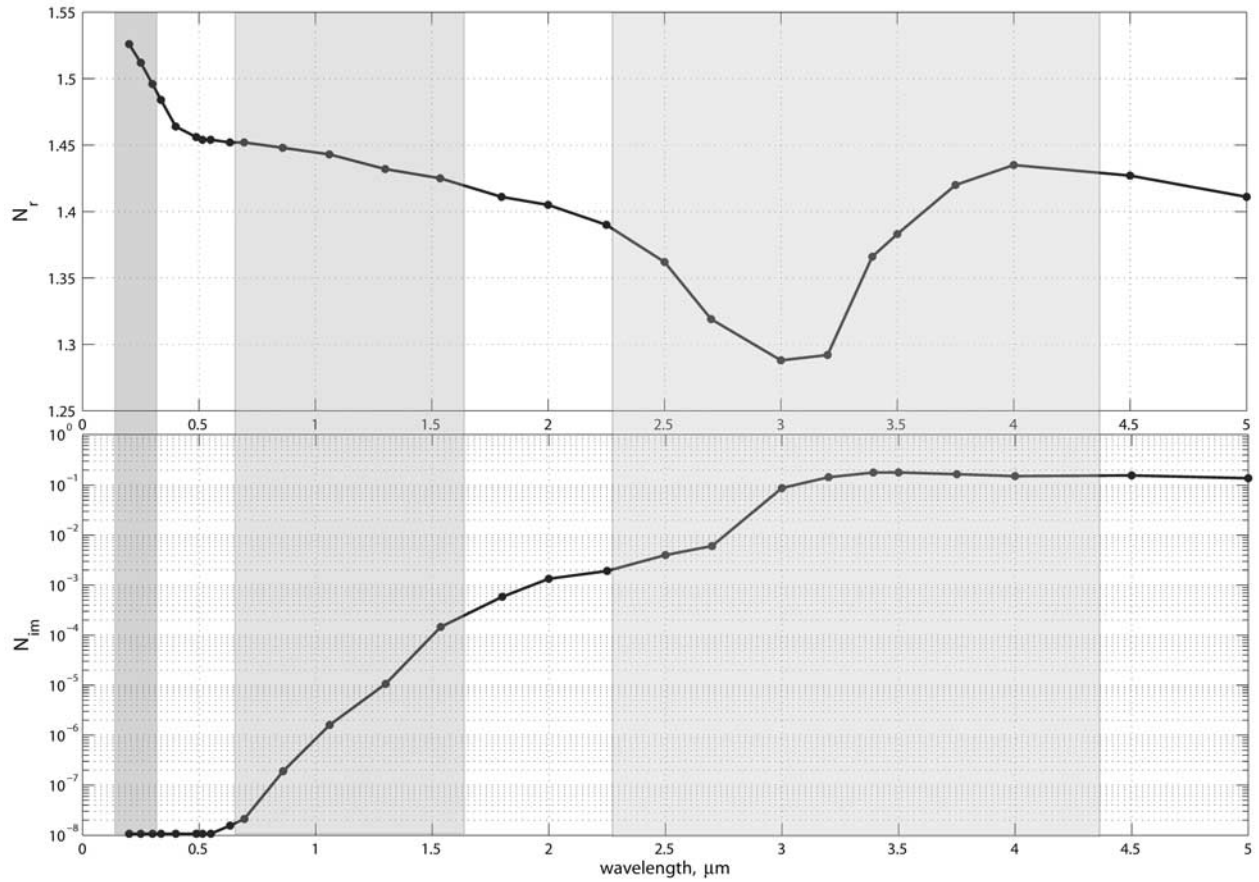


**Figure 5.** Refraction index model ( $T = 215$  K) assuming 75%  $\text{H}_2\text{SO}_4$  spherical particles and classical Mie theory [Hummel *et al.*, 1988] in the wavelength range covered by the SPICAV/SOIR instrument. The boxes show the spectral windows of the instrument; dark gray box for the SPICAV-UV channel, gray for the SPICAV-IR channel, and light gray for the SOIR channel.

where  $N(z)$  is the particle total number density at altitude  $z$  and  $Q(r; \lambda)$  is the extinction cross section at wavelength  $\lambda$ . A lognormal distribution has been used to describe the size distribution of particles of radius  $r$  in the Venus upper haze:

$$f(r; r_g, \sigma_g) = \text{const} \times r^{-1} \exp\left(-\frac{(\ln r - \ln r_g)^2}{2 \ln^2 \sigma_g}\right) \quad (3)$$

where  $r_g$  and  $\sigma_g$  are the mean radius and variance.

[28] The calculation of the extinction cross section  $Q(r, \lambda)$  is based on Mie theory, assuming that the upper haze aerosols are composed of 75%  $\text{H}_2\text{SO}_4$  aqueous spherical particles, whose refractive index is derived from Hummel *et al.* [1988] for  $T = 215$  K (see Figure 5). The spectral ranges probed by the three channels of the SPICAV/SOIR instrument are also indicated in Figure 5 and clearly show the complementarity between them.

[29] The aerosol extinction coefficients  $\beta$  derived for each of the sampled wavelength ranges (i.e., for one channel) are then normalized to a reference wavelength  $\lambda_r$ :

$$\beta_n^e = \frac{\beta(z; \lambda)}{\beta(z; \lambda_r)} \quad (4)$$

This reference is chosen as  $\beta$  (852.7 nm) for SPICAV IR and  $\beta$  (250 nm) for SPICAV UV. In the case of SOIR, the reference value corresponds to the higher wave number probed, since the four spectral intervals in one occultation are not always the same.

[30] Finally, an estimation of the particle radius was obtained as described in the paper by Bingen *et al.* [2003], by fitting the normalized experimental aerosol extinctions  $\beta_n^e$ , obtained from equation (4), to their corresponding theoretical values:

$$\beta^t(r_g, \sigma_g, \lambda) = \int_0^{+\infty} f(r; r_g, \sigma_g) Q(r; \lambda) dr \quad (5)$$

The fit was obtained by minimization of the merit function:

$$M(r_g, \sigma_g; z) = \sum_{i=1}^4 \left[ \frac{\beta_n^e(z; \lambda_i) - \beta_n^t(r_g, \sigma_g; \lambda_i)}{\Delta \beta_n^e(z; \lambda_i)} \right]^2 \quad (6)$$

This leads to the determination of the aerosol parameters  $\sigma_g(z)$  and  $r_g(z)$ , where  $\Delta \beta$  is the 1-sigma error on the retrieved extinction coefficients. Once the radius that gives the best fit at each altitude has been extracted, the



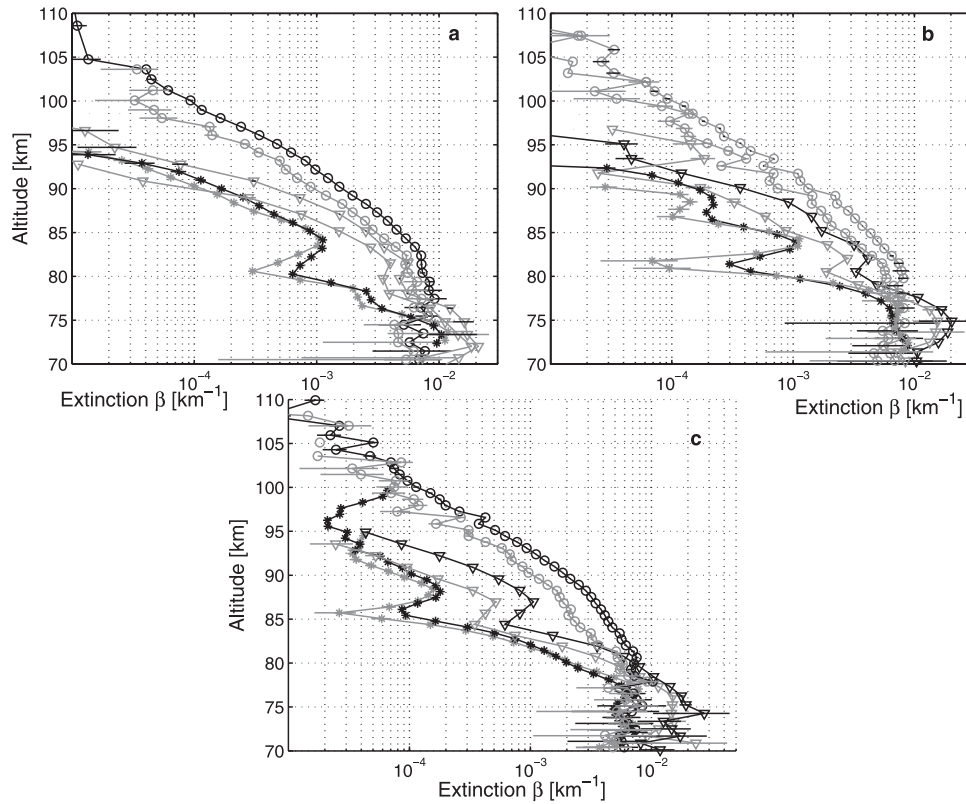


**Figure 6.** Vertical profiles of the  $\beta$  extinction coefficient obtained with the three channels of the SPICAV/SOIR instrument for the orbits (a) 485, (b) 486, and (c) 487. The extinction was obtained from data acquired with SPICAV-UV at 220 nm (black circles), SPICAV-UV at 300 nm (gray circles), SPICAV-IR at 757 nm (black inverted triangles), SPICAV-IR at 1553 nm (gray inverted triangles), on Figure 6a with SOIR at 2560 nm (gray asterisks) and SOIR at 3978 nm (black asterisks), and on Figure 6b and Figure 6c with SOIR at 2345 nm (gray asterisks) and SOIR at 3682 nm (black asterisks).

corresponding model of particle number density  $N(z)$  that best fits the data can also be found.

## 5. Results

### 5.1. Vertical Profiles of Aerosol Extinctions

[31] The extinction coefficients  $\beta$  retrieved as described in section 4.1 are plotted in Figure 6 for the selected orbits, when all three channels of the instrument were measuring simultaneously. For clarity,  $\beta$  for only two wavelengths per channel of the SPICAV/SOIR instrument are shown.

[32] The general trend is a decrease of the extinction with increasing altitude except when aerosol layers are observed. This phenomenon was more pronounced at longer wavelengths (SOIR channel) than at shorter wavelengths (SPICAV-UV). It could indicate the presence of particles with a size larger than the wavelengths of the UV channel ( $>300$  nm), which is less sensitive to such particles. In general, less temporal variability of the  $\beta$  coefficient was observed in the UV than in the IR.

[33] These aerosol layers have been observed in several occultations, mainly during summer 2007, showing temporal and/or spatial variations in terms of the altitude of the layer (Figure 7). Figure 7 illustrates the apparition and the displacement of such layers observed with the SOIR channel in the upper haze during orbits 482 and 484 to 487. While the layers were almost not visible in the UV, they

were also detected with the SPICAV-IR channel (Figure 6), yet a small difference in the altitude of the layer is observed between the SPICAV-IR and the SOIR channels. This can be explained by a weak accuracy of the calibration of the FOV of the SPICAV-IR channel. For orbit 482, the extinction coefficient, for the four spectral windows investigated during the solar occultation, increased fairly smoothly with decreasing altitude. In addition, the extinction showed little spectral dependency; that is, the extinction is very similar for the four diffraction orders. In contrast, for orbits 484 to 487, one or two layers appeared in the extinction profiles in which extinction decreased with decreasing altitude before it increased further (Figure 7). The altitude of the layers varied from orbit to orbit, they were located at  $\sim 82$  km and  $\sim 74$  km for orbit 484,  $\sim 78$  km and maybe  $\sim 74$  km for orbit 485 and, at  $\sim 84$  km and  $\sim 78$  km for orbit 486 and at  $\sim 83$  km and maybe  $\sim 72$  km for orbit 487. Moreover, the spectral dependency of the extinction was greater for these occultations than for the one during orbit 482 and was strikingly higher within the layers than at other altitudes (Figure 7). For example, in orbit 486, at an altitude of 78.5 km, there is about 1 order of magnitude for  $\beta$  between diffraction order 171 ( $\sim 4 \times 10^{-5} \text{ km}^{-1}$ ) and order 121 ( $\sim 3 \times 10^{-4} \text{ km}^{-1}$ ). We are currently retrieving temperature, density and pressure from these peculiar orbits, as a layer was not observed in all occultations, to see if there is any correlation with the observed variations of the layer.

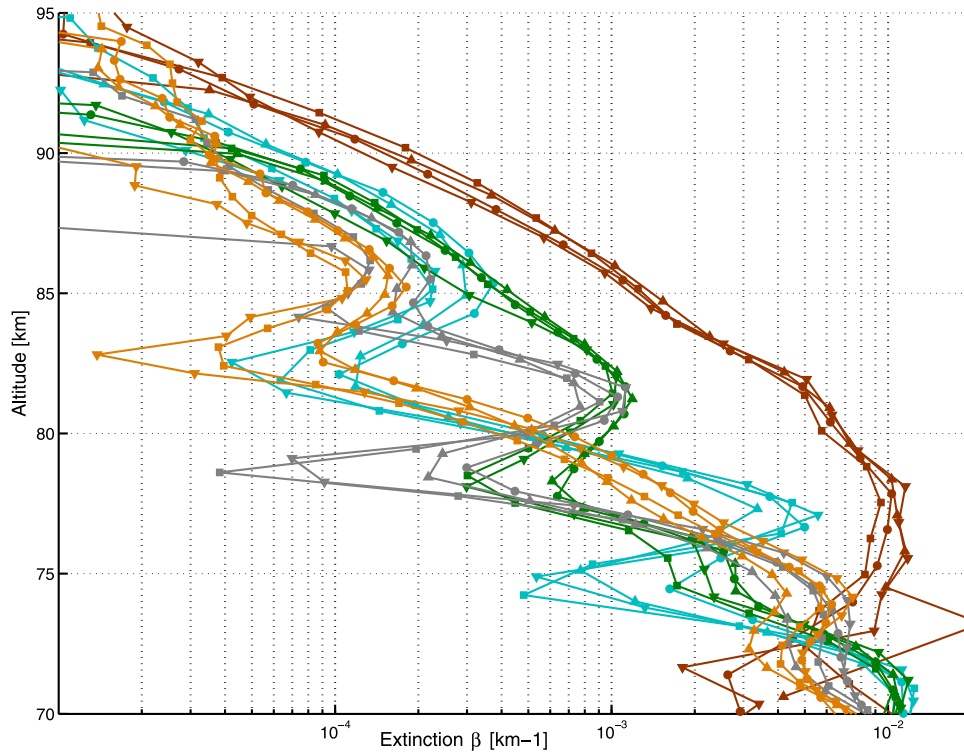


**Figure 7.** Temporal variation of a layer in the extinction profiles observed with the SOIR channel. Extinction coefficients in function of the altitude for orbit 482 (brown), diffraction orders 111 (circles), 121 (triangles), 137 (squares), 171 (inverted triangles); orbit 484 (blue), diffraction orders 125 (circles), 149 (triangles), 172 (squares), 180 (inverted triangles); orbit 485 (green), diffraction orders 112 (circles), 119 (triangles), 149 (squares), 174 (inverted triangles); orbit 486 (gray), diffraction orders 121 (circles), 149 (triangles), 171 (squares), 190 (inverted triangles); and orbit 487 (orange), diffraction orders 121 (circles), 149 (triangles), 171 (squares), 190 (inverted triangles).

[34] Detached layers of aerosols were already observed in the past above the Venus clouds [Lane and Opstbaum, 1983]. It is preliminary here to speculate on the mechanisms of formation of such layers but gravity waves are known to create stratified layers in the atmosphere. Recently, internal gravity waves have been identified in the lower and upper clouds of Venus [Peralta et al., 2008].

## 5.2. Retrieval of Particle Size

[35] The use of the three channels allowed us to investigate a broad range of wavelengths in the UV and the IR and to make use of the spectral dependence of the extinction (Figure 5) to infer aerosol size(s). It is worth mentioning that the simultaneous use of the three channels in the solar occultation mode was not possible at the beginning of the VEX mission but through a programming adaptation, it has been in operation for about 1 year. This means that for the earlier measurements, aerosol characterization has to be performed from data acquired by two channels (SOIR and SPICAV-IR). We therefore make first an attempt to derive independently particle size(s) and number densities of the Venusian upper haze from the extinction coefficients obtained for each of the three channels of the instrument. This analysis is illustrated using a number of orbits with coordinated solar occultations and using the method described in section 4.3, i.e., by fitting the aerosol extinction

curve with a Mie theory model (equation (5)). A lognormal distribution (equation (3)) was assumed where  $\sigma_g$  was variable for SPICAV-UV and fixed to 0.1 for SPICAV-IR and SOIR (similar particle sizes were found for a fixed variance of 0.2 or of 0.3, data not shown), and the refractive indices of  $\text{H}_2\text{SO}_4$  compiled by Hummel et al. [1988] was used.

[36] Figure 8 shows the vertical size distribution of the particles for solar occultations performed during orbits 485, 486, and 487. The channels cannot discriminate particles with a radius higher than the wavelength at which the data were acquired, i.e., for these particular orbits, a maximal radius of  $0.3 \mu\text{m}$  for SPICAV-UV, of  $1.6 \mu\text{m}$  for SPICAV-IR and of  $3.7 \mu\text{m}$  for SOIR.

[37] The data obtained with the UV channel indicate the presence of particles with a radius increasing from  $\sim 0.1 \mu\text{m}$  at 100 km up to  $\sim 0.3 \mu\text{m}$  at 75 km (Figure 8). The vertical distribution for this channel exhibits low variability from one orbit to another.

[38] From the SOIR and SPICAV-IR channels, the vertical distribution of particle size is limited to altitudes comprised between 70 km and 90–95 km. The radii determined with both channels are in fairly good agreement and are comprised between 0.4 and  $1.0 \mu\text{m}$ . Particles of  $\sim 1 \mu\text{m}$  were detected at  $\sim 74$ – $77$  km of altitude during all orbits. For each orbit analyzed here, the maxima in the

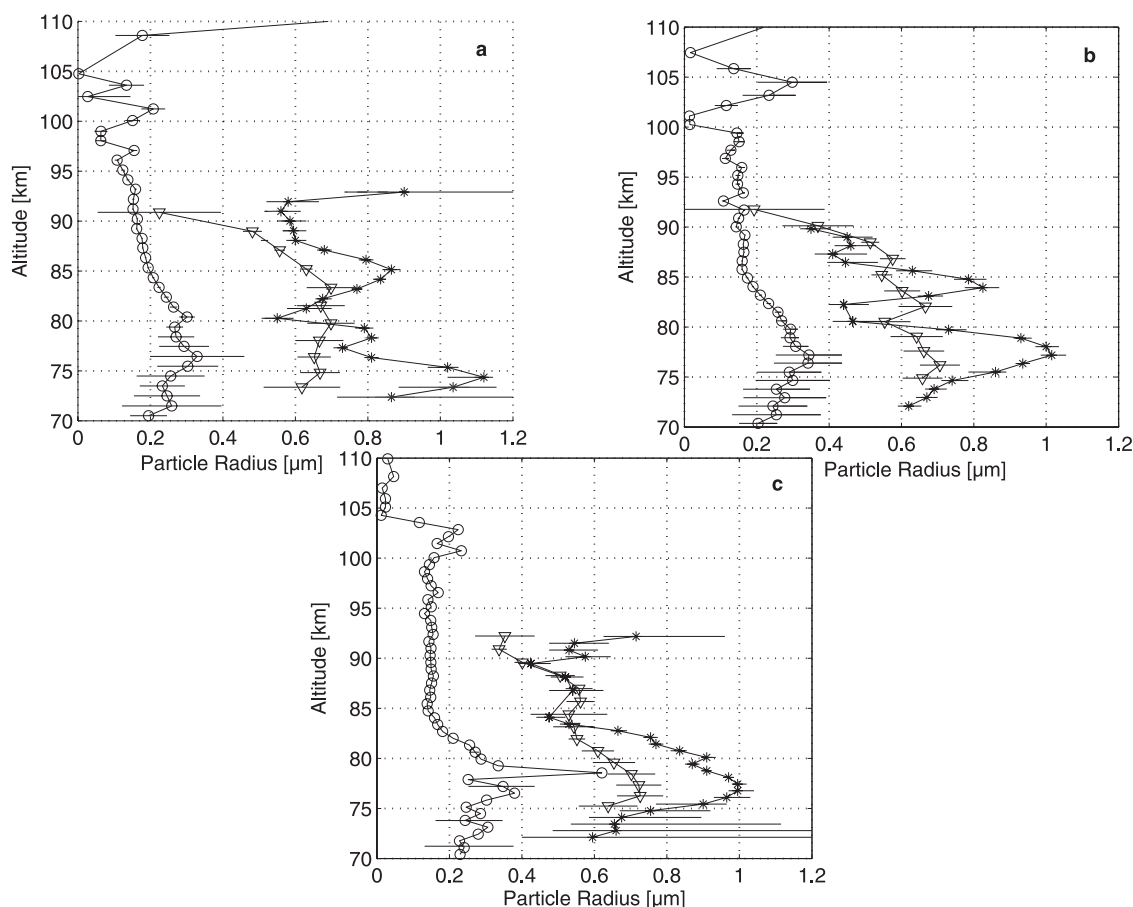


**Figure 8.** Vertical distributions of particle size for orbits (a) 485, (b) 486, and (c) 487. Radii derived from normalized extinction values obtained at 2 wavelengths with the SPICAV-UV channel (circles), at 10 wavelengths with the SPICAV-IR channel (inverted triangles), and at 4 wavelengths with the SOIR channel (asterisks).

vertical particle size distribution (Figure 8) correlate with the maxima of the extinction vertical profiles (Figure 6). The aerosol layers also exhibited temporal and/or spatial variations in terms of the size of the particles within the layer, from 0.4 up to 1.0  $\mu\text{m}$  radius.

[39] The particle sizes found with the UV channel in this study are in good agreement with values obtained previously. *Sato et al.* [1996] compiled Venus cloud and haze properties deduced from Pioneer Venus, Venera, and Vega mission results. *Sato et al.* [1996] reported haze particles in the north polar region of  $r_g = 0.25 \mu\text{m} \pm 0.05 \mu\text{m}$  and  $\sigma_g = 0.25 \mu\text{m} \pm 0.05$ , while *Esposito* [1983] identified particles of  $r_g = 0.2 \mu\text{m}$  and *Kawabata et al.* [1980] estimated haze particles of  $r_g = 0.23 \mu\text{m} \pm 0.04 \mu\text{m}$  and  $\sigma_g = 0.18 \mu\text{m} \pm 0.1$ . They all refer to an altitude range comprised between 70 and 90 km, called the upper haze. However, our measurements tend to suggest that the two modes found in the upper clouds (properties summarized by *Esposito* [1983]), usually defined as mode 1 ( $r_g = 0.2 \mu\text{m}$ ) and mode 2 ( $r_g = 1.0 \mu\text{m}$ ), are still both present at altitudes higher than 70.0 km. Earlier works reported that modes 1 and 2 only coexist in the upper cloud region (55–70 km) or below and that only mode 1 is found above. Whether the merging of these two modes account for only one global

mode of particles or two separate distributions cannot be firmly established on the basis of this analysis alone.

### 5.3. Total Particle Number Density

[40] Figure 9 shows the particle number densities derived in the UV spectral range for aerosol particles of about 0.1–0.3  $\mu\text{m}$  size from the SPICAV-UV channel and in the IR for aerosol particles of about 0.4–1.0  $\mu\text{m}$  size from the SPICAV-IR and the SOIR channels depending on the altitude. SPICAV-UV measurements lead to mode 1 particle number density between 10 and 30  $\text{cm}^{-3}$  below 90 km, decreasing at higher altitudes. These values are 1 order of magnitude lower than those reported by *Esposito* [1983] but more consistent with the measurements from Pioneer Venus limb scans [*Lane and Opstbaum*, 1983] at northern midlatitude, close to the orbit latitudes analyzed in this paper (Table 1).

[41] Number density for the larger particles (mode 2) decreases smoothly from 10 to 15  $\text{cm}^{-3}$  at 70 km down to less than 1  $\text{cm}^{-3}$  at 90 km. It is important to mention that the results obtained for the two IR channels are very comparable although they were calculated from independent data sets, yet from simultaneous measurements. The values found at about 70 km, which is the boundary between the upper cloud and the upper haze, is close to, yet smaller than the one reported by *Esposito* [1983] for

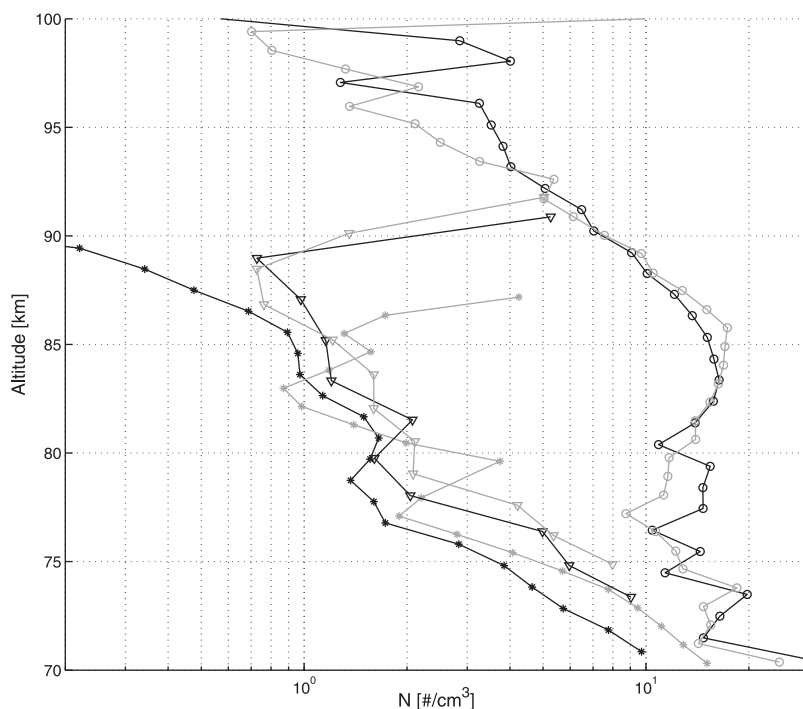


**Figure 9.** Vertical profiles of the particle total number density in the Venus upper haze during two successive orbits of Venus Express. The radius of particles found by fitting normalized extinction to a haze model allowed derive  $N$  for mode 1 particles with the SPICAV-UV channel (circles),  $N$  for mode 2 particles with the SPICAV-IR channel (inverted triangles), and  $N$  for mode 2 particles with the SOIR channel (asterisks) during orbit 485 (black) and orbit 486 (gray).

mode 2 particles in the upper cloud region, i.e.,  $50 \text{ cm}^{-3}$ . Nevertheless, the values found in this restricted analysis (only three orbits) should be taken with caution and are indicative of an order of magnitude for the number density for mode 2 particles. A systematic multichannel retrieval is currently ongoing. The combination of extinction coefficients obtained from UV up to mid-IR and the use of a bimodal particle size distribution will probably allow retrieving unique aerosols parameters and solving the discrepancies between nadir [Esposito, 1983] and limb viewing [Lane and Opstbaum, 1983].

## 6. Conclusion

[42] The number of orbits analyzed was restricted for this paper, aimed at proving the capability of the SPICAV/SOIR instrument on board Venus Express to characterize the upper haze of Venus' atmosphere. The ability of the instrument since March 2007 to perform simultaneous solar occultations with the three channels will allow us to investigate the upper haze in greater detail in the future and to plan solar occultations specifically for this purpose. This could be achieved by making use of the full spectral range of the instrument, from 170 nm up to  $4 \mu\text{m}$ , by choosing appropriate, regularly spread wavelengths for each channel, and by taking maximum advantage of the spectral dependency of the extinction studied in this paper.

[43] One of the main advantages of the solar occultation technique is the high vertical resolution and in comparison

with nadir viewing, a much longer optical path resulting in an improved sensitivity. In addition, data collected at terminators could lead to a better understanding of the known morning/evening asymmetry of the upper haze [Esposito, 1983].

[44] The determination of the particles sizes performed for this paper was made independently for the different channels of the SPICAV/SOIR instrument. The first results look promising for further analysis of the aerosols in the mesosphere of Venus as, in the future, the radii of particles could be retrieved in one single minimization of the merit function (see section 4.3) from the extinction coefficients obtained with the three channels. This study demonstrated the existence of at least two types of particles, one type with a radius comprised between  $\sim 0.1$  and  $0.3 \mu\text{m}$  as inferred by the UV channel and the second type, detected in the IR, with a radius varying between  $\sim 0.4$  and  $1 \mu\text{m}$  depending on the altitude. Therefore, the model describing the upper haze on Venus should include a bimodal population for putting together the three channels in retrieving particle sizes from the extinction profiles. To our knowledge, this is the first time that the existence of mode 2 particles at altitudes above 70 km in the atmosphere of Venus is shown. It was found independently for the two IR channels of the SPICAV/SOIR instrument, giving strong evidence for its existence.

[45] Our measurements also showed the high temporal variability of the aerosol loading in the Venus mesosphere. The SPICAV/SOIR is well suited to study the vertical distribution of the different types of aerosols, as well as such temporal and latitudinal variability.



[46] **Acknowledgments.** The research program was supported by the Belgian Federal Science Policy Office and the European Space Agency (ESA-PRODEX program contracts C 90268, 90113, and 17645). The Russian team acknowledges RFBR grant 06-02-72563.

## References

- Bertaux, J. L., D. Nevejans, O. Korablev, E. Villard, E. Quémerais, E. Neefs, F. Montmessin, F. Leblanc, J. P. Dubois, and E. Dimarellis (2007), SPICAV on Venus Express: Three spectrometers to study the global structure and composition of the Venus atmosphere, *Planet. Space Sci.*, 55(12), 1673–1700, doi:10.1016/j.pss.2007.01.016.
- Bertaux, J.-L., A. C. Vandaele, V. Wilquet, F. Montmessin, R. Dahoo, E. Villard, O. Korablev, and A. Fedorova (2008), First observation of 628 CO<sub>2</sub> isotopologue band at 3.3 μm in the atmosphere of Venus by solar occultation from Venus Express, *Icarus*, 195(1), 28–33, doi:10.1016/j.icarus.2008.01.001.
- Bingen, C., F. Vanhellefont, and D. Fussen (2003), A new regularized inversion method for the retrieval of stratospheric aerosol size distributions applied to 16 years of SAGE II data (1984–2000): Method, results and validation, *Ann. Geophys.*, 21, 797–804.
- Esposito, L. W. (1983), The clouds and hazes on Venus, in *Venus*, edited by D. M. Hunten et al., pp. 484–564, Univ. of Ariz., Tucson.
- Fedorova, A., et al. (2008a), HDO and H<sub>2</sub>O vertical distribution and isotopic ratio in the Venus mesosphere by Solar Occultation at Infrared spectrometer on board Venus Express, *J. Geophys. Res.*, 113, E00B22, doi:10.1029/2008JE003146.
- Fedorova, A. A., O. I. Korablev, J.-L. Bertaux, A. V. Rodin, F. Montmessin, D. A. Belyaev, and A. Reberac (2008b), Solar infrared occultations by SPICAM experiment on Mars-Express: Simultaneous measurement of the vertical distributions of H<sub>2</sub>O, CO<sub>2</sub> and aerosol, *Icarus*, 200, 96–117.
- Hummel, J. R., E. P. Shettle, and D. R. Longtin (1988), A new background stratospheric aerosol model for use in atmospheric radiation models, *AFGL-TR-88-0166*, Air Force Geophys. Lab., Hanscom Air Force Base, Mass.
- Kawabata, K., D. L. Coffeen, J. E. Hansen, W. A. Lane, M. Sato, and L. D. Travis (1980), Cloud and haze properties from Pioneer Venus polarimetry, *J. Geophys. Res.*, 85(A13), 8129–8140, doi:10.1029/JA085iA13p08129.
- Korablev, O., et al. (2006), SPICAM IR acousto-optic spectrometer experiment on Mars Express, *J. Geophys. Res.*, 111, E09S03, doi:10.1029/2006JE002696.
- Lane, W. A., and R. Opstbaum (1983), High altitude Venus haze from Pioneer Venus limb scans, *Icarus*, 54, 48–58, doi:10.1016/0019-1035(83)90071-4.
- Mahieux, A., et al. (2008), In-flight performance and calibration of SPICAV SOIR on board Venus Express, *Appl. Opt.*, 47(13), 2252–2265, doi:10.1364/AO.47.002252.
- Montmessin, F., et al. (2006a), Sub-visible CO<sub>2</sub> ice clouds detected in the mesosphere of Mars, *Icarus*, 183, 403–410, doi:10.1016/j.icarus.2006.03.015.
- Montmessin, F., E. Quémerais, J. L. Bertaux, O. Korablev, P. Rannou, and S. Lebonnois (2006b), Stellar occultations at UV wavelengths by the SPICAM instrument: Retrieval and analysis of Martian haze profiles, *J. Geophys. Res.*, 111, E09S09, doi:10.1029/2005JE002662.
- Nevejans, D., et al. (2006), Compact high-resolution space-borne echelle grating spectrometer with AOTF based on order sorting for the infrared domain from 2.2 to 4.3 micrometer, *Appl. Opt.*, 45(21), 5191–5206, doi:10.1364/AO.45.005191.
- Peralta, J., R. Hueso, A. Sánchez-Lavega, S. Pérez-Hoyos, G. Piccioni, O. Lanciano, P. Drossart, and t.V.-V.E. team (2008), Characterization of gravity waves in the upper and lower clouds of Venus using VIRTIS-VEX images, *Geophys. Res. Abstr.*, 3, Abstract EPSC2008-A-00095.
- Quémerais, E., J.-L. Bertaux, O. Korablev, E. Dimarellis, C. Cot, B. R. Sandel, and D. Fussen (2006), Stellar occultations observed by SPICAM on Mars Express, *J. Geophys. Res.*, 111, E09S04, doi:10.1029/2005JE002604.
- Sato, M., L. D. Travis, and K. Kawabata (1996), Photopolarimetry analysis of the Venus atmosphere in polar regions, *Icarus*, 124, 569–585, doi:10.1006/icar.1996.0231.
- Svedhem, H., et al. (2007), Venus Express—The first European mission to Venus, *Planet. Space Sci.*, 55(12), 1636–1652, doi:10.1016/j.pss.2007.01.013.
- Titov, D. V., et al. (2006), Venus Express science planning, *Planet. Space Sci.*, 54(13–14), 1279–1297, doi:10.1016/j.pss.2006.04.017.
- Vandaele, A. C., et al. (2008), Composition of the Venus mesosphere measured by SOIR on board Venus Express, *J. Geophys. Res.*, 113, E00B23, doi:10.1029/2008JE003140.
- Wilquet, V., A. Mahieux, A. C. Vandaele, V. I. Perevalov, S. A. Tashkun, A. Fedorova, O. Korablev, F. Montmessin, R. Dahoo, and J.-L. Bertaux (2008), Line parameters for the 01111–00001 band of <sup>12</sup>C<sup>16</sup>O<sup>18</sup>O from SOIR measurements of the Venus atmosphere, *J. Quant. Spectrosc. Radiat. Transfer*, 109, 895–905, doi:10.1016/j.jqsrt.2007.12.021.

J.-L. Bertaux, F. Montmessin, and E. Villard, Service d'Aéronomie du CNRS, BP3, F-91371, Verrières-le-Buisson, France.

R. Drummond, A. Mahieux, A. C. Vandaele, and V. Wilquet, Belgian Institute for Space Aeronomy, 3 Avenue Circulaire, B-1180 Brussels, Belgium. (valerie.wilquet@aeronomie.be)

A. Fedorova and O. Korablev, Space Research Institute, 84/32 Profsoyuznaya Street, 117997, Moscow, Russia.